Theor Appl Climatol
DOI 10.1007/s00704-008-0042-4

ORIGINAL PAPER

Multi-scale variability patterns in NCEP/NCAR reanalysis sea-level pressure

S. M. Barbosa · M. E. Silva · M. J. Fernandes

Received: 9 October 2006 / Accepted: 25 April 2008

Abstract Atmospheric pressure varies within a wide range of scales and thus a multi-scale description of its variability is particularly appealing. In this study, a scale-by-scale analysis of the global sea-level pressure field is carried out from reanalysis data. Wavelet-based analysis of variance is applied in order to describe the variability of the pressure field in terms of patterns representing the contribution of each scale to the overall variance. Signals at the seasonal scales account for the largest fraction of sea-level pressure variance (typically more than 60%) except in the Southern Ocean, in the Equatorial Pacific and in the North Atlantic. In the Southern Ocean and over the North Atlantic, high-frequency signals contribute to a considerable fraction (30–50%) of the overall variance in sea-level pressure. In the Equatorial Pacific, large-scale variability, associated with ENSO, contributes up to 40% of the total variance.

1 Introduction

The variability of the global sea-level pressure field is a topic of considerable interest in the analysis of the Earth's climate. Variations in atmospheric pressure are associated with several climatic phenomena including the monsoons (Singh et al. 1996), the North Atlantic Oscillation (Barnston and Livezey 1987; Hurrell 1995; Rogers 1997; Marshall et al. 2001) or the El Niño/Southern Oscillation (ENSO; Walker and Bliss 1932; Bjerknes 1969; Wang and Fiedler 2006, for a review). The variability of atmospheric pressure at the global scale is thus of significant importance in climate analysis.

The atmospheric pressure field is often analysed through space-time methods such as empirical orthogonal functions (e.g. Von Storch and Zwiers (1999)). EOF techniques are very effective for dimensionality reduction and for the extraction of dominant modes of variability, but offer only a limited solution when the aim is the description of the variability of the field, since features may be physically relevant while not explaining a large fraction of the field's overall variance.

An alternative approach consists in the individual analysis of each pressure time series. This allows the description of the features of the pressure series at each gridpoint, independently of its contribution to the variability of the overall field, but has been applied mainly in terms of low-frequency or seasonal patterns. Gillett et al. (2003) examined low-frequency changes in sea-level pressure by computing linear trends from both observations and climate models. The seasonal cycle of sea-level pressure has been analysed by Yashayaeva and Zveryaevb (2001) over the oceans of the Northern Hemisphere. Such analysis use parametric approaches for the estimation of linear trends and seasonal amplitudes, thus assuming the same fixed pattern over the whole period. An improved description of low-frequency and seasonal variability requires flexible, often non-parametric, approaches in order to extract realistic patterns of variability and identify changes over the observed period (e.g. Bograd et al. 2002; Barbosa et al. 2004, 2008). Furthermore, since the pressure field exhibits spatial and temporal variability within a wide range of scales, a multi-scale description of its variability is more appealing than focusing only on low-frequency or seasonal patterns. Recently, Zhao and Moore (2006) analysed the

S. M. Barbosa (✉) · M. E. Silva · M. J. Fernandes
Departamento de Matematica Aplicada, Faculdade de Ciencias,
Universidade do Porto,
Rua Campo Alegre, 687,
4169-007 Porto, Portugal
e-mail: susana.barbosa@fc.up.pt

variability in the Northern Hemisphere sea-level pressure field through a frequency-dependent approach and showed the existence of distinct features at inter-annual, inter-decadal and multi-decadal timescales.

In this study, a multi-scale analysis of the global sea-level pressure field is carried out from reanalysis data. The wavelet domain is a powerful non-parametric framework for the scale-based analysis of climate data (e.g. Lau and Weng (1995); Kumar and Foufoula-Georgiou (1997); Torrence and Compo (1998); Higuchi et al. (1999); Sonechkin et al. (1999); Barbosa et al. (2005); Percival (2008)). Here, wavelet analysis of variance is applied in order to obtain a flexible scale-by-scale decomposition of the variability of the global pressure field, with no need of further assumptions on the form of the variability patterns at each scale.

2 Data

Sea level pressure (SLP) data from the NCEP/NCAR reanalysis project (Kalnay et al. 1996; Kistler et al. 2001) are considered. The analysed dataset comprises monthly SLP values on a regular 2.5º global grid (144×73=10,512 gridpoints) from January 1948 to December 2007 (720 months). Monthly SLP values are averages of instantaneous values at four reference hours (0,6,12 and 18) over each month.

The average SLP field, obtained by computing for each gridpoint the SLP mean over the whole 60-years period, is shown in Fig. 1. The dominant features of global sea level pressure are visible in the average field, including the high gradient region at the edge of the Antarctica continent associated with the katabatic winds, high pressure systems such as the Azores high and the Siberian High, and persistent low pressure regions such as the Icelandic Low, the Aleutian Low and the southern area between 50ºS and 80ºS.The anomaly field, obtained by subtracting from the original dataset the average SLP field, is considered hereafter.

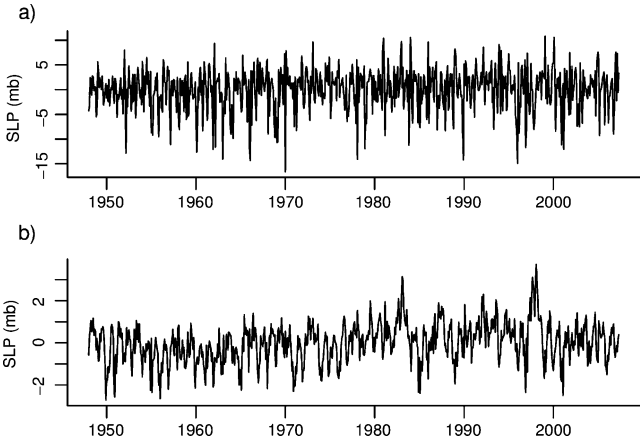

Fig. 2 Time series of sea level pressure (SLP) at gridpoints **a** 340° E 40° N (northeast Atlantic) and **b** 240° E 0° N (eastern equatorial Pacific)

3 Analysis

The wavelet analysis procedure is illustrated in the following section for sea-level pressure time series at sample gridpoints (shown in Fig. 1). The variability patterns resulting from the application of the methodology to all gridpoints and over the whole period (60 years) are presented in the section 3.2, which is followed by the section 3.3 where the investigation is performed by a running-window wavelet analysis of variance.

3.1 Wavelet analysis

The wavelet analysis is illustrated here for SLP time series at gridpoints 340ºE 40ºN and 240ºE 0ºN (Fig. 2). The cumulative periodograms for these series are displayed in Fig. 3. The time series from the northeast Atlantic (340ºE

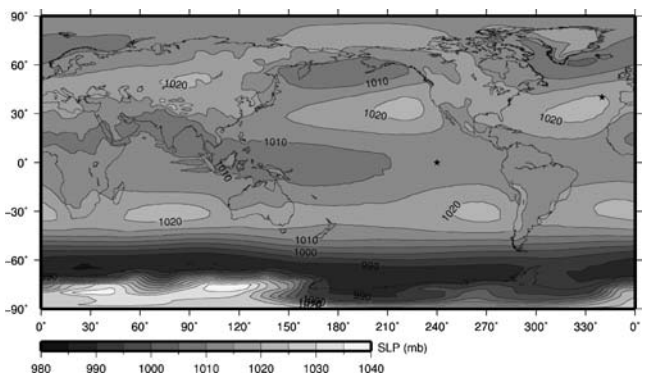

Fig. 1 Mean SLP field. The *stars* indicate the gridpoints for which the analysis is illustrated

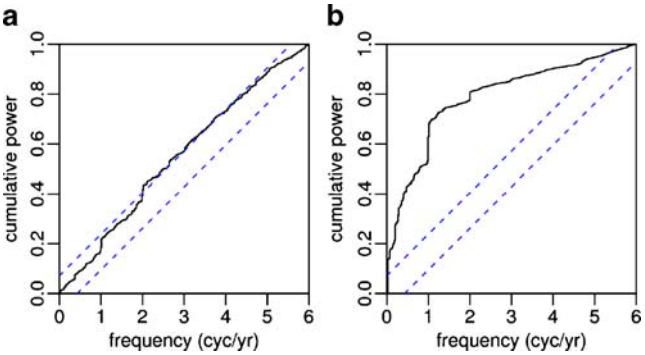

Fig. 3 Cumulative periodograms for sample SLP time series: **a** 340° E 40° N; **b** 240° E 0° N. *Dashed lines* represent 95% confidence interval for white noise

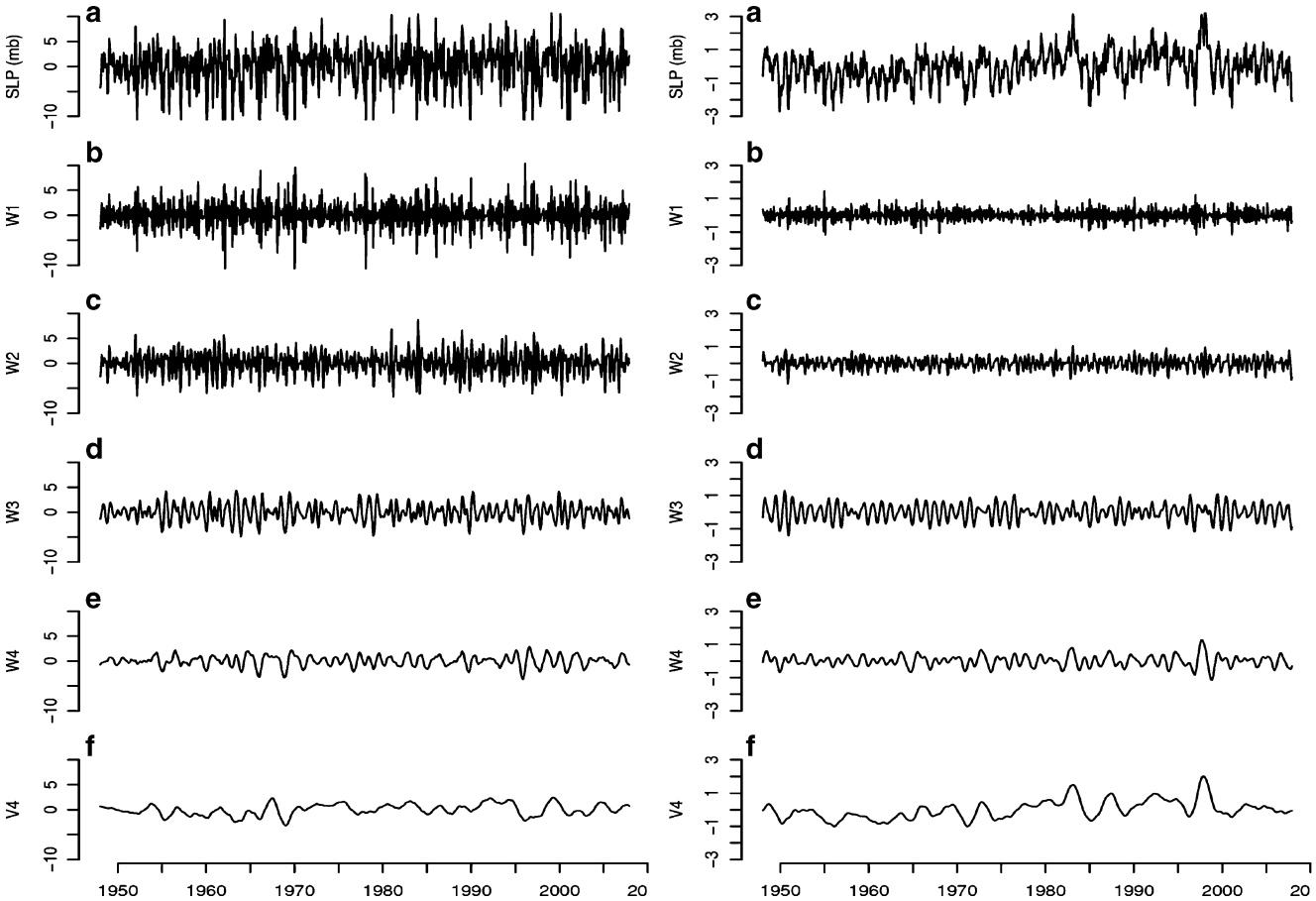

Fig. 4 Maximal overlap discrete wavelet transform for sample SLP time series at 340° E 40° N (*left*) and 240° E 0° N (*right*). From top to bottom: **a** original time series, **b**–**e** wavelet coefficients associated with scales of $\tau_j=2^{j-1}$ months, j=1,...,4 and **f** scaling coefficients associated with scales of $2^{j=4}$ months and higher

40ºN) exhibits an almost flat periodogram with the dominant periodicity, only slightly above noise level, being at the semi-annual frequency. In contrast, the periodogram for the SLP time series from the eastern equatorial Pacific (240ºE 0ºN) exhibits a sharp transition at the annual frequency and a secondary one at the semi-annual frequency, indicating the presence of a strong annual cycle and a weaker semi-annual harmonic. Furthermore, the periodogram also shows considerable spectral content at the lowest frequencies, indicating the presence of long-term features in the temporal pattern of the time series.

The maximal overlap discrete wavelet transform (Percival and Mojfeld 1997; Lindsay et al. 1996; Percival and Walden 2000) is applied for a four-level scale-based decomposition of the time series. The wavelet transformation is based on a Daubechies least asymmetric filter of width L=8 (Daubechies 1988) with periodic boundary conditions. The decomposition yields four sub-series of wavelet coefficients, corresponding to band-pass filtered series with approximate pass-band $1/2^{j+1}\leq f\leq 1/2^{j}$, j=1,...,4 and a sub-series of scaling coefficients reflecting large-scale changes (Fig. 4). The wavelet transformation yields a scale-based decomposition from fine to coarse scale of the original time series (Fig. 4a) into sequences of wavelet coefficients associated with scales of $\tau_j=2^{j-1}$ months, j=1,...,4 (Fig. 4b–e) and a sequence of scaling coefficients associated with scales of $2^{j=4}$ months and higher (Fig. 4f). The first wavelet sub-series (at scale τ_1) captures high frequency variability (changes from one month to the next). Due to the band-pass nature of the discrete wavelet transform, the annual component is captured at the wavelet scale τ_3 (8-16 month periods) and the semi-annual component is captured at the wavelet scale τ_2 (4-8 month periods). Inter-annual variability is reflected by scale τ_4.

The empirical wavelet variance for each scale is computed from the corresponding sub-series of wavelet coefficients (Percival 1995; Serroukh et al. 2000). The contribution of each individual scale to the overall variability is assessed by considering the wavelet variance at each scale, normalised by the sum of the wavelet variances at all scales. The results obtained are displayed in Fig. 5. The wavelet variance values agree with the features observed in the periodograms of the time series, namely the dominance of the semi-annual over the annual

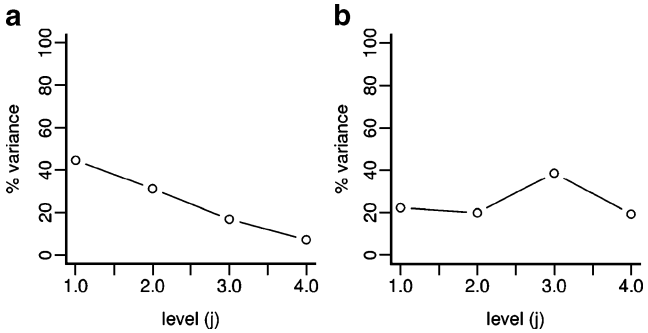

Fig. 5 Normalised wavelet variance (%) for sample SLP time series at gridpoints: **a** 340° E 40° N and **b** 77.5° E 35° N

cycle for the time series at 340ºE 40ºN and the strong contribution of the annual cycle to the overall variability of the time series at 240ºE 0ºN. The wavelet variance provides a scale-based measure of the contribution of each scale to the total variability, with no need of further assumptions on the shape of the temporal patterns at each scale (for example, the often unrealistic assumption of a pure sinusoidal cycle for the periodic components).

3.2 Variability patterns

The analysis described in the previous section is carried out for all the 10,512 gridpoints of the 2.5° reanalysis global grid. For the time series at each gridpoint, the MODWT decomposition is performed and the normalised wavelet variance is computed from the corresponding wavelet coefficients. Maps of SLP variability patterns are obtained by plotting the normalised wavelet variance values representing the contribution of each scale to the total variance (Fig. 6). High-frequency variability (corresponding to changes from month to month) is typically below 40% of the total variance, lower (<10%) in continental areas and higher (>20%) over the Southern Ocean, North Atlantic, North Pacific and Western Europe (Fig. 6a). The semiannual signal is stronger over the North Atlantic, particularly in the Caribbean area, in the northwestern Pacific and over the Southern Ocean, explaining 20–40% of the variance in sea level pressure (Fig. 6b). The annual signal is, unsurprisingly, the dominant contribution to sea-level pressure variance at most locations, explaining more than 70% of the time series variance over continental areas, and a lower fraction, 20–40%, over the oceans (Fig. 6c). Variability at the largest scale is considerably lower, below 10% over most of the globe, except in the Equatorial Pacific, where the contribution is higher, ascending to more than 30% in the Indonesian region. The spatial pattern is consistent with variability associated with the ENSO phenomenon.

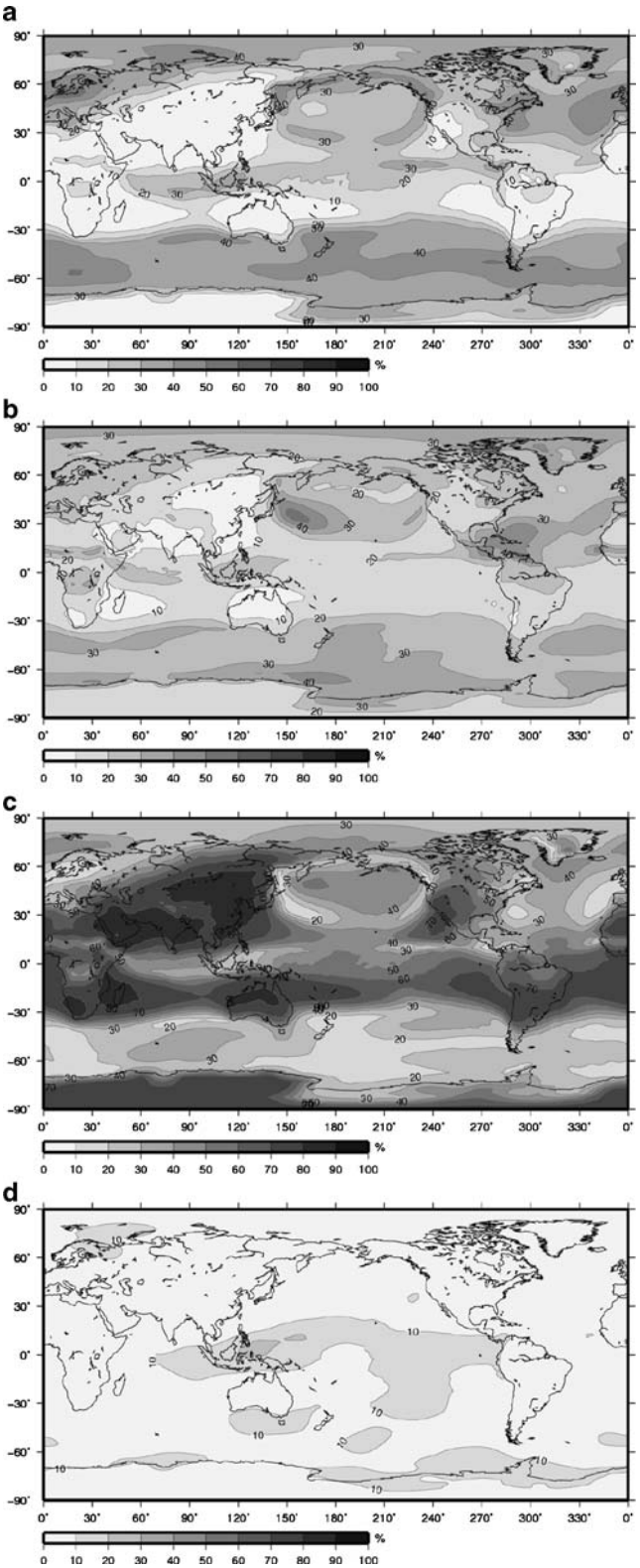

Fig. 6 Maps of normalised wavelet variance (%) from SLP time series: **a** scale τ_1 (high-frequency); **b** scale τ_2 (semi-annual); **c** scale τ_3 (annual); **d** scale τ_4 (inter-annual)

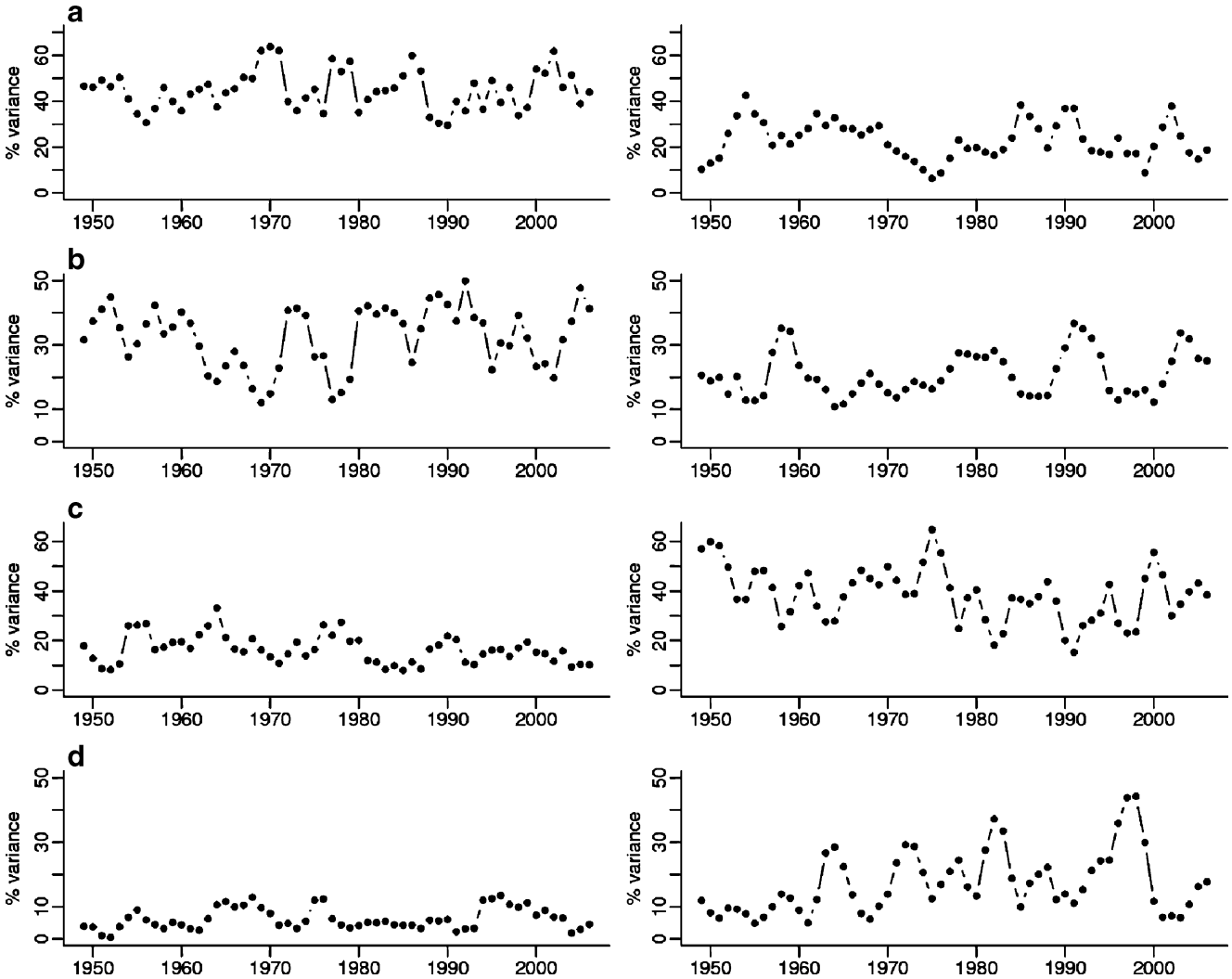

Fig. 7 Empirical normalised wavelet variance over a 3-year running window for sample SLP time series at 340° E 40° N (*left*) and 240° E 0° N (*right*). From top to bottom: **a** scale τ_1 (high-frequency); **b** scale τ_2 (semi-annual); **c** scale τ_3 (annual); **d** scale τ_4 (inter-annual)

3.3 Changes in variability patterns

Temporal changes in the variability patterns are investigated by carrying out a running-window wavelet analysis. For each gridpoint, the time series of sea-level pressure data is decomposed via the maximal overlap discrete wavelet transform (see section 3.2 and Fig. 4). However, instead of computing from this decomposition, the wavelet variance for each scale over the whole 1948–2007 period, the empirical wavelet variance is computed, from the same components, over a 3-year running window. The resulting sequences of normalised wavelet variance values at each scale are shown for sample SLP gridpoints in Fig. 7. For the sample gridpoint in the north-east Atlantic, the contribution of high-frequency, annual and inter-annual signals to the overall variability is more stable through time, while the contribution of semi-annual signals exhibits some larger fluctuations over the observation period. For the gridpoint in the eastern equatorial Pacific, the most obvious feature is the clear increase in the relative importance of the inter-annual scale associated with ENSO events.

The analysis described above is repeated for all the 10,512 gridpoints and summarised through the first EOF mode of the running wavelet variance sequences at each scale (Fig. 8). Regarding high-frequency variability, the first EOF mode for scale τ_1 explains only 12.4% of the variance in running-window wavelet variance sequences and reflects a smaller contribution of high-frequency variability in the 1970s and an enhancement of high-frequency signals around 1985 and 2000. The dominant EOF at scale τ_2, explaining 14.3% of the variance, represents an increase in the contribution of semi-annual signals to the overall variability of the sea-level pressure field in northern Europe and in the Atlantic storm track area, and a decrease of the relative importance of semi-annual variability in western Antarctica. At the annual scale

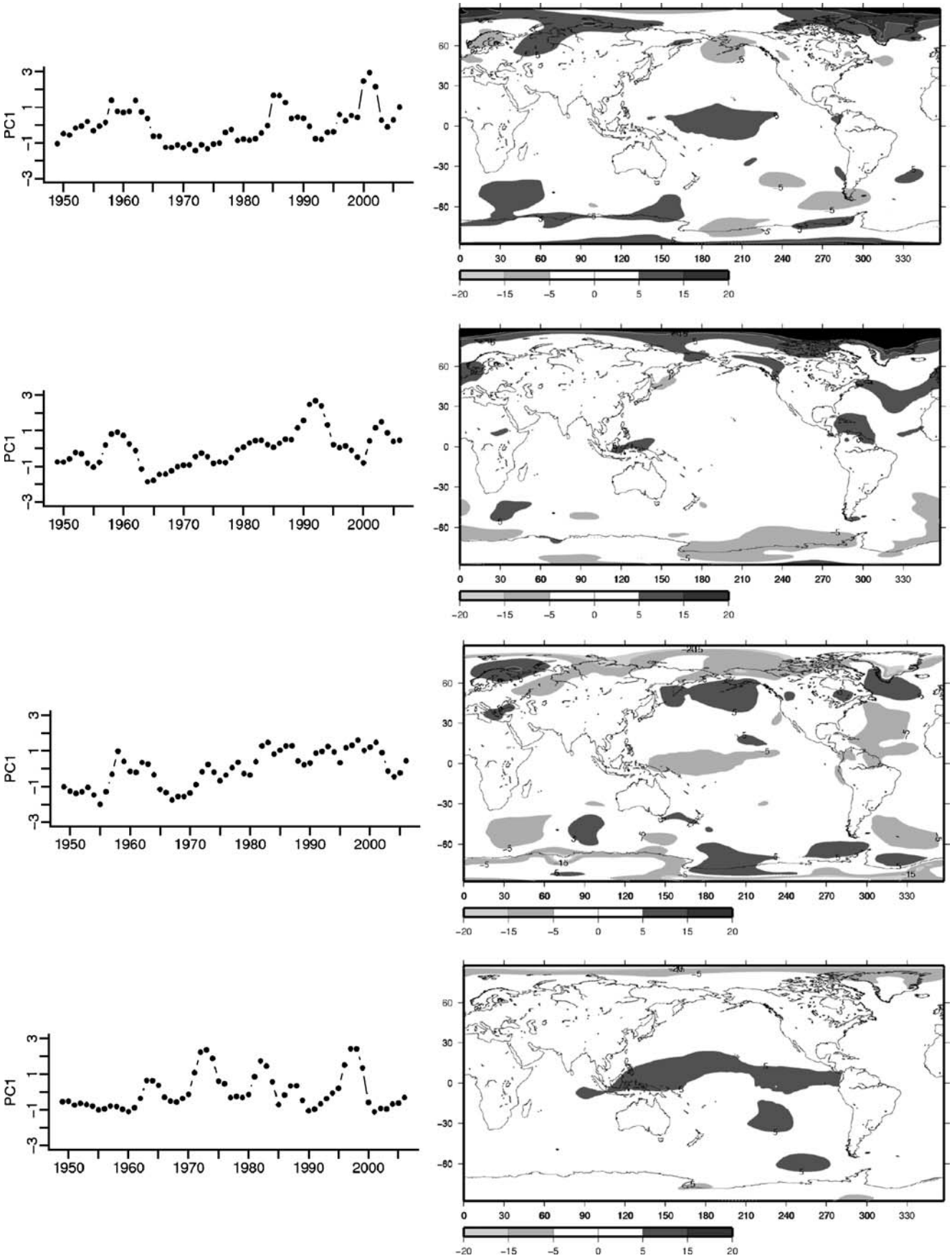
PC1
3
1
−1
−3
1950
1960
1970
1980
1990
2000
60
30
0
−30
−60
0
30
60
90
120
150
180
210
240
270
300
330
−20
−15
−5
0
5
15
20

◀ **Fig. 8** Temporal (*left*) and spatial (*right*) patterns of the first EOF of running wavelet variance sequences. From top to bottom: **a** scale τ_1 (high-frequency); **b** scale τ_2 (semi-annual); **c** scale τ_3 (annual); **d** scale τ_4 (inter-annual)

τ_3, the first EOF explains 15.7% of the variance and exhibits a dipolar pattern over the North Atlantic, the North Pacific and northern Europe. The temporal pattern exhibits a positive trend towards increasing relative importance of the annual signal in the overall variability of atmospheric pressure.

The most clear pattern appears at the inter-annual scale τ_4, with the dominant EOF mode explaining 39% of the variance. Furthermore, both the temporal and the spatial patterns of the dominant EOF mode show a clear ENSO signature, indicating that inter-annual variability in the global pressure field is mainly driven by this climatic phenomenon.

4 Conclusions

Since climate fields exhibit spatial and temporal variability within a wide range of scales, the description of climate variability on a scale-by-scale basis is particularly appealing. Here, a multi-scale analysis of SLP variability is carried out through a wavelet-based analysis of variance. The approach yields a scale-based description of the sea-level pressure field in terms of the contribution of each scale to the overall variance.

Signals at the seasonal scales (annual, semi-annual) account for the largest fraction of SLP variability, typically more than 60%, almost everywhere; the exceptions are the Southern Ocean, the Equatorial Pacific and the North Atlantic, for which signals at seasonal scales explain only ~50% of the overall variability. In the Southern Ocean and over the North Atlantic (particularly at mid-latitudes), high-frequency signals account for a large fraction (30–50%) of the overall variance in sea-level pressure. In the Equatorial Pacific, large-scale variability (apparently associated with ENSO) contributes up to 40% of the total variance.

The spatial patterns of variability obtained here for the seasonal scales (τ_2 and τ_3) are similar to the patterns obtained by Yashayaeva and Zveryaevb (2001) for the amplitudes of annual and semi-annual harmonics of SLP in the north Pacific and North Atlantic Oceans from COADS data. This is somewhat expected, since due to the approximate pass-band nature of the discrete wavelet transform, semi-annual and annual signals are captured at scales τ_2 and τ_3 respectively, and the amplitude of the seasonal cycles is directly related to the corresponding variance. The main difference (and advantage) of the analysis carried out here is that the wavelet-based methodology allows for non-purely sinusoidal signals, thus providing a more flexible and realistic description of the seasonal patterns. Furthermore, the wavelet decomposition yields time-varying seasonal components, with non-constant amplitude and phase, thus enabling the investigation of changes in the temporal structure of the components.

Changes in the variability structure of the SLP field have been investigated through a running window wavelet analysis of variance. The results clearly show a ENSO signature at the inter-annual scale, indicating that the contribution of inter-annual signals to the overall variability in atmospheric pressure in the equatorial Pacific area increases with the occurrence of ENSO events. Furthermore, the relative importance of high-frequency, semi-annual and annual signals to the overall variability of the global pressure field exhibits decadal trends in confined areas of the north Atlantic, North Pacific, Northern Europe and Antarctica. Some of these variations in the relative importance of specific scales of variability can result from artificial signals in the reanalysis dataset rather than actual variations in the pressure field. Reanalysis data are particularly sensitive to bias introduced by changes in the observing system, resulting in artificial trends in reanalysis fields, particularly in the tropics and in the southern hemisphere (Hines et al. 2000; Marshall and Harangozo 2000; Marshall 2002; Bromwich and Fogt 2004; Hertzog et al. 2006). Still, such eventual bias in the reanalysis dataset cannot explain the increase in the contribution of the inter-annual scale associated with ENSO events. By yielding nonparametric and flexible descriptions of the variability patterns, the approach presented in this study allowed the investigation of temporal changes in the variability patterns and the detection of a clear ENSO signature at the inter-annual scale. The wavelet variance is an efficient tool for the multi-scale analysis of large space-time climate datasets and for the investigation of corresponding temporal changes.

Acknowledgements This work has been supported by FCT (Fundação para a Ciência e Tecnologia, grant SFRH/BPD/23992/2005) and by program POCTI through the Centro de Investigação em Ciências Geo-espaciais (CICGE). NCEP Reanalysis data provided by the NOAA/OAR/ESRL PSD, Boulder, Colorado, USA, from their Web site at http://www.cdc.noaa.gov/. Data analysis was performed with R software (http://R-project.org) and with R-package waveslim from B. Whitcher.

References

Barbosa SM, Fernandes MJ, Silva ME (2004) Nonlinear sea level trends from European tide gauge records. Ann Geophys 22:1465–1472

Barbosa SM, Silva ME, Fernandes MJ (2005) Wavelet analysis of the Lisbon and Gibraltar North Atlantic Oscillation winter indices. Int J Climatol 26:581–593

Barbosa SM, Silva ME, Fernandes MJ (2008) Changing seasonality in North Atlantic coastal sea level from the analysis of long tide gauge records. Tellus 60A:165–177

Barnston AG, Livezey RE (1987) Classification, seasonality and persistence of low frequency atmospheric circulation patterns. Mon Weather Rev 115:1083–1126

Bjerknes J (1969) Atmospheric teleconnections from the equatorial Pacific. Mon Weather Rev 97:163–172

Bograd S, Schwing F, Mendelssohn R, Green-Jessen P (2002) On the changing seasonality over the North Pacific. Geophys Res Lett 29. DOI 10.1029/2001GL013790

Bromwich DH, Fogt RL (2004) Strong trends in the skill of the ERA-40 and NCEP-NCAR reanalyses in the high and midlatitudes of the Southern Hemisphere, 1958–2001. J Climate 17:4603–4619

Daubechies I (1988) Orthonormal bases of compactly supported wavelets. Commun Pure Appl Math 41:909–996

Gillett NP, Zwiers FW, Weaver AJ, Stott PA (2003) Detection of human influence on sea level pressure. Nature 422:292–294

Hertzog A, Basdevant C, Vial F (2006) An Assessment of ECMWF and NCEP-NCAR reanalyses in the Southern Hemisphere at the end of the Presatellite Era: results from the EOLE experiment (1971–72). Mon Weather Rev 134:3367–3383

Higuchi K, Huang J, Shabbar A (1999) A wavelet characterisation of the North Atlantic Oscillation variation and its relationship to the North Atlantic sea surface temperature. Int J Climatol 19:1119–1129

Hines KM, Bromwich DH, Marshall GJ (2000) Artificial surface pressure trends in the NCEP-NCAR reanalysis over the Southern Ocean and Antarctica. J Climate 13:3940–3952

Hurrell J (1995) Decadal trends in the NAO: regional temperatures and precipitation. Science 269:676–679

Kalnay E, Kanamitsu M, Kistler R, Collins W, Deaven D, Gandin L, Iredell M, Saha S, White G, Woollen J, Zhu Y, Chelliah M, Ebisuzaki W, Higgins W, Janowiak J, Mo KC, Ropelewski C, Wang J, Leetmaa A, Reynolds R, Jenne R, Joseph D (1996) The NCEP/NCAR 40-year reanalysis project. Bull Am Meteorol Soc 77:437–471

Kistler R, Kalnay E, Collins W, Saha S, White G, Woollen J, Chelliah M, Ebisuzaki W, Kanamitsu M, Kousky V, Van den Dool H, Jenne R, Fiorino M (2001) The NCEP-NCAR 50-year reanalysis: monthly means CD-ROM and documentation. Bull Am Meteorol Soc 82:247–267

Kumar P, Foufoula-Georgiou E (1997) Wavelet analysis for geophysical applications. Rev Geophys 35:385–412

Lau KM, Weng H (1995) Climate signal detection using wavelet transform: how to make a time series sing. Bull Am Meteorol Soc 76:2391–2402

Lindsay RW, Percival DB, Rothrock DA (1996) The discrete wavelet transform and the scale analysis of the surface properties of sea ice. IEEE T Geosci Remote Sens 34:771–787

Marshall GJ (2002) Trends in Antarctic geopotential height and temperature: a comparison between radiosonde and NCEP-NCAR reanalysis data. J Climate 15:659–674

Marshall GJ, Harangozo SA (2000) An appraisal of NCEP/NCAR reanalysis MSLP data variability for climate studies in the South Pacific. Geophys Res Lett 27:3057–3060

Marshall J, Kushnir Y, Battisti D, Chang P, Czaja A, Dickson R, Hurrell J, McCartney M, Saravanan R, Visbeck M (2001) North Atlantic climate variability: phenomena, impacts and mechanisms. Int J Climatol 21:1863–1891

Percival DB (1995) On the estimation of the wavelet variance. Biometrika 82:619–631

Percival DB (2008) Analysis of geophysical time series using discrete wavelet transforms: an overview. In: Donner R, Barbosa SM (eds) Nonlinear time series analysis in the geosciences: applications in climatology, geodynamics, and solar-terrestrial physics. Springer, Berlin

Percival DB, Mojfeld H (1997) Analysis of subtidal coastal sea level fluctuations using wavelets. J Am Stat Assoc 92:868–880

Percival DB, Walden A (2000) Wavelet methods for time series analysis. Cambridge University Press, Cambridge

Rogers J (1997) North Atlantic storm track variability and its association to the NAO and climate variability of Northern Europe. J Climate 10:1635–1647

Serroukh A, Walden AT, Percival DB (2000) Statistical properties and uses of the wavelet variance estimator for the scale analysis of time series. J Am Stat Assoc 95:184–196

Singh D, Bhadram CVV, Goyal S, Mandal GS (1996) Relationship between North Pacific atmospheric pressure variations and Indian monsoon rainfall. Theor Appl Climatol 54:117–123

Sonechkin DM, Astafyeva NM, Datsenko NM, Ivachtchenko NN, Jakubiak B (1999) Multiscale oscillations of the global climate system as revealed by wavelet transform of observational data time series. Theor Appl Climatol 64:131–142

Torrence C, Compo G (1998) A practical guide to wavelet analysis. Bull Am Meteorol Soc 79:61–78

Von Storch H, Zwiers FW (1999) Statistical analysis in climate research. Cambridge University Press, Cambridge

Walker GT, Bliss E (1932) World weather V. Mem R Meteorol Soc 4:53–84

Wang C, Fiedler PC (2006) ENSO variability and the eastern tropical Pacific: a review. Prog Oceanogr 69:239–266

Yashayaeva I, Zveryaevb IM (2001) Climate of the seasonal cycle in the North Pacific and the North Atlantic oceans. Int J Climatol 21:401–417

Zhao H, Moore GWK (2006) Timescale dependency of spatial patterns in the variability of the Northern Hemisphere winter SLP field. Geophys Res Lett 33:L13710. DOI 10.1029/2006GL026090